Final Draft

of the original manuscript

Renk, O.; Tkadletz, M.; Kostoglou, N.; Gunduz, I.; Fezzaa, K.; Sun, T.; Stark, A.; Doumanidis, C.; Eckert, J.; Pippan, R.; Mitterer, C.; Rebholz, C.:

Synthesis of bulk reactive Ni–Al composites using high pressure torsion.

In: Journal of Alloys and Compounds. Vol. 857 (2021) 157503.

First published online by Elsevier: 15.10.2020

https://dx.doi.org/10.1016/j.jallcom.2020.157503

Synthesis of Bulk Reactive Ni-Al Composites Using High Pressure Torsion

Oliver Renk[1,2*], Michael Tkadletz[2], Nikolaos Kostoglou[2], Ibrahim Emre Gunduz[3], Kamel Fezzaa[4], Tao Sun[4°], Andreas Stark[5], Charalabos C. Doumanidis[6,7], Jürgen Eckert[1,2], Reinhard Pippan[1], Christian Mitterer[2], Claus Rebholz[2,8]

[1] Erich Schmid Institute of Materials Science, Austrian Academy of Sciences, 8700 Leoben, Austria

[2] Department of Materials Science, Montanuniversität Leoben, 8700 Leoben, Austria.

[3] Department of Mechanical and Aerospace Engineering, Naval Postgraduate School, Monterey, CA 93943, USA.

[4] Advanced Photon Source, Argonne National Laboratory, Lemont, IL 60439, USA.

[5] Institute of Materials Research, Helmholtz-Zentrum Geesthacht, 21502, Geesthacht, Germany.

[6] Office of the Provost, Nazarbayev University, 010000 Astana, Kazakhstan.

[7] College of Engineering & Computer Science, Vin University, Hanoi, Vietnam

[8] Department of Mechanical and Manufacturing Engineering, University of Cyprus, 1678 Nicosia, Cyprus.

[*] Corresponding author: oliver.renk@oeaw.ac.at (Oliver Renk)

° current address, Department of Materials Science and Engineering, University of Virginia, Charlottesville, VA

Abstract

Self-propagating exothermic reactions, for instance in the nickel-aluminum (Ni-Al) system, have been widely studied to create high performance intermetallic compounds or for in-situ welding. Their easy ignition once the phase spacing is reduced below the micron scale, makes top-down methods like high-energy ball milling, ideal to fabricate such reactive nanostructures. A major drawback of ball milling is the need of a sintering step to form bulk pieces of the reactive material. However, this is not possible, as the targeted reactions would already proceed. Therefore, we investigate the ability of high pressure torsion as an alternative process, capable to produce bulk nanocomposites from powder mixtures. Severe straining of powder mixtures with a composition of 50 wt.% Ni and 50 wt.% Al enables fabrication of self-reactive bulk samples with microstructures similar to those obtained from ball milling or magnetron sputtering. Samples deformed at ambient temperature are highly reactive and can be ignited significantly below the Al melting point, finally predominantly consisting of Al_3Ni_2 and Al_3Ni, independent of the applied strain. Although the reaction proceeds first at the edge of the disk, the strain gradient present in the disks does not prevent reaction of the whole sample.

Keywords: high pressure torsion; nanocomposites; ignition; self-propagation reaction; nickel aluminides

1. Introduction

The Ni-Al system has been used extensively to study metallo-thermic reactions for combustion synthesis of high temperature NiAl and Ni_3Al intermetallic alloys, *in situ* welding and structural energetic materials [1–10]. Magnetron sputter deposition has become a useful method to produce intermetallic reactives with multiple targets sequentially depositing nanoscale layers [11–14]. This method allows to synthesize Ni-Al multilayered foils having a highly controlled microstructure with individual layer thicknesses down to 10 nm [14]. Consequently, the typical sluggish reaction kinetics in macroscale mixtures of Ni-Al can be accelerated by reducing the dimensions of the constituents down to the submicron- or nanoscale [15–25]. However, major drawbacks of this method are the inherent slow deposition rates, typically on the order of a few angstroms per second, and the high costs of the process. Therefore, alternative approaches that allow to overcome these limitations have been explored. Scalable top-down processes were mostly targeted, where severe degrees of deformation are applied to initially coarse structures to refine them down to the nanoscale. A frequently used method for fabricating energetic mixtures is high-energy ball milling (HEBM) [16–18,26]. This approach uses a planetary ball mill to apply high inertial forces to the milling media (e.g. stainless-steel balls) that repeatedly impact and deform the powder mixtures. This results in a significant refinement of the phase dimensions and yields micronscale composite powders consisting of nanoscale features which are nearly as reactive as multilayered foils. However, the milled powders would have to be consolidated for further use, which is an issue as conventional sintering can already start the intermetallic phase reactions occurring at approximately 500 K, or disrupt the nanoscale structure due to grain growth, which retards the reaction kinetics. Furthermore, contamination from the milling agents, milling media and the container is always present. Another approach is accumulative roll bonding (ARB), where metal sheets are rolled and folded repeatedly to decrease the individual layer thicknesses through plastic work, while maintaining the starting

sheet thickness [27]. For 50 % thickness reduction conventionally applied in ARB, the layer thickness reduces by $^{1}/_{2^{N}}$, with N the number of rolling passes applied. Thus, even when starting already with metal foils (typical thicknesses of several tens of micrometers), huge numbers of rolling passes are required to achieve nanoscale structures comparable to HEBM. Moreover, this only holds true in case of ideal co-deformation of the individual phases, which is hardly possible for material combinations having substantially different mechanical properties such as Ni and Al. For such material combinations, uniform refinement of the individual phases is hard to accomplish, as the softer Al layers preferentially deform. This can cause thinning and eventual necking of these layers, as frequently observed [28,29]. To reduce the layer dimensions below 100 nm and ensure a high degree of reactivity, more than 50 folding and rolling passes for the Ni-Al system seem to be necessary [29]. Thus, ARB can take many rolling passes to realize a high degree of refinement. Lubricant contamination from the rolls can be problematic as well and requires the use of sacrificial layers that have to be replaced at each cycle or cleaning of the sheets before restacking. Other methods include cold spraying, where the powders impact a substrate at high velocities to form a deposit [30,31]. However, heat generation from powder particle deformation can already initiate early reactions or diffusion and also for this method the issue of the strength mismatch between the Al and Ni powders prevails. These limitations motivate to explore new cost efficient methods that have the potential to generate uniform nanocomposites and allow to process large amounts of consolidated material while minimizing contamination.

One promising approach in that direction is high pressure torsion (HPT), which is capable to produce nanostructured materials or nanocomposites not only from bulk precursors but also from individual powder mixtures [32,33]. HPT uses cylindrical specimens which are compressed under high hydrostatic pressures between two hardened steel anvils. Subsequently, high shear strains are applied to consolidate and refine the starting powder particles down to

the nanoscale. However, as enormous strain levels can be easily applied, mechanical alloying or the formation of intermetallic phases already during the HPT process have been reported [33–36], which could impede the targeted reactions. Formation of the Al_3Ni phase already during HPT of Ni-Al powder mixtures has been observed indeed for sufficiently large strains and deformation temperatures [37]. Thus the applied strain and deformation temperature need to be kept as low as possible, to avoid intermetallic phase formation already upon processing. In addition, the strain gradient naturally present along the radius of the HPT disk could result for composite materials in microstructural gradients and hence different reaction kinetics. This could eventually deteriorate the ignition behavior, the reaction rates or prevent reaction of the whole disk in case of the Ni-Al system. Therefore, the present study aims to explore the use and feasibility of HPT for fabricating bulk reactive Ni-Al composites. To understand the refinement process as well as the influence of the nanostructure on the ignition behavior and the reaction sequence, the samples are characterized using scanning electron microscopy (SEM), X-ray diffraction (XRD) as well as thermal analysis. As a whole, the results demonstrate that HPT provides indeed an efficient method to fabricate bulk and highly self-reactive specimens.

2. Experimental Methods

To synthesize bulk self-reactive samples, elementary nickel (Ni, 3-7 µm particle size, 99.9 % purity) and aluminum (Al, 5 µm average particle size, 99.5 % purity) metal powders with an overall composition of 50 wt.% (~ 70 at.% Al), respectively, were blended. Subsequently, they were cold consolidated and refined by applying severe torsional strains using a quasi-constrained HPT device [38]. The metallic powder mixtures were filled into the cavity of the HPT anvil, which was surrounded by a thin copper ring. The copper ring had a diameter larger than the actual cavity to ensure enough powder quantity for the subsequent deformation step (see schematics in Fig. 1). After compression at room temperature with a nominal pressure of

7.8 GPa, the entire copper ring was removed and the sample was subsequently deformed under the same nominal pressure. The samples, having a diameter of 8 mm and a thickness, *t*, of about 0.8 mm, were subjected to various numbers of rotations, *n*, (i.e. 0, 0.5, 1, 2, 3, 5 and 8) at ambient temperature, corresponding to different equivalent von Mises strains, ε_{vM}, according to Eq. 1 [39], where *r* denotes the sample radius. Compared to earlier studies on the Ni-Al system (e.g. Ref. [37]), comparably low strains were deliberately chosen to prevent mechanically induced intermixing or phase formation upon processing, consequently complicating sample ignition. The rotation rate (ω = 0.2 rot min^{-1}) was kept at a low level to avoid self-heating of the samples, as indicated by earlier in-depth studies [40].

$$\varepsilon_{vM} = \frac{2\,r\,\pi\,n}{\sqrt{3}t} \qquad \text{Eq. (1)}$$

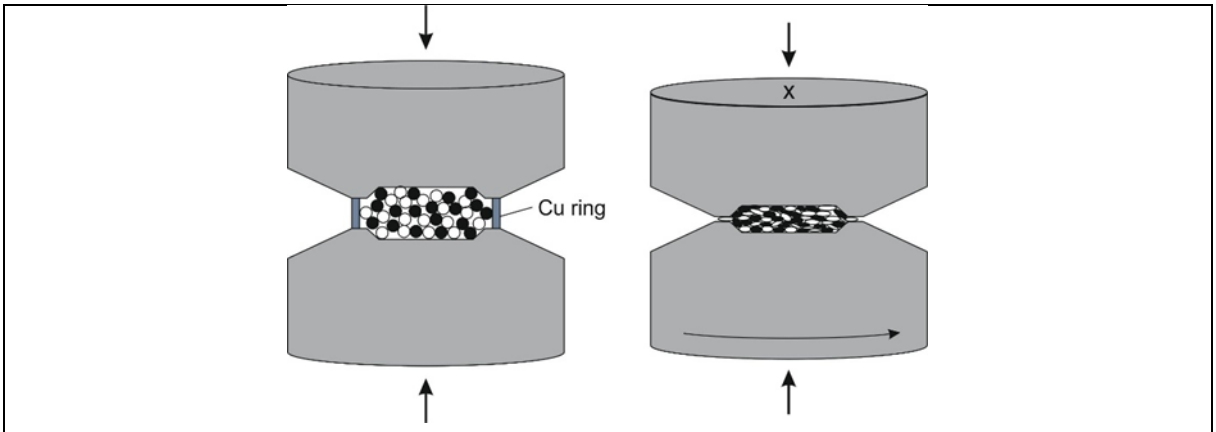

Fig. 1. Schematics showing the synthesis of the Ni-Al nanocomposites using a high pressure torsion device. Images are not to scale.

The resulting microstructures and phases of the various as-deformed samples as well as the reaction-induced changes were analyzed in detail using SEM, differential scanning calorimetry (DSC), XRD as well as separate scanning and *in situ* synchrotron XRD measurements on selected samples. Because the spacing and morphology of the precursor phases Ni and Al as well as the heating rate could possibly affect the occurring reactions and final product phases

[10,13,41], XRD phase analysis was not only performed on the DSC annealed samples but also on a similar batch of ignited ones. Together with the *in situ* ignition experiment, this allowed to identify the according reaction pathways and their influence on external variables, such as heating rate or phase spacing. Samples for microstructural characterization in the SEM were prepared by conventional grinding and polishing followed by a final mechano-chemical polishing step using colloidal silica. All samples were analyzed in a Zeiss LEO 1525 field emission gun SEM. The images were taken in radial (RAD) direction of the HPT disk at a radius of approximately 3 mm. For definition of the three principal axis of the HPT disks studied, see the inset image in Fig. 3.

The SEM images of the consolidated and HPT deformed Ni and Al powders, exhibiting self-similar granular and lamellar features across various magnification scales, were analyzed regarding their fractal dimension [42] via box-counting algorithms implemented by image processing software [43]. The fractal dimension reflects the multi-scale geometric wiggledness (or 3D spatial complexity) of Ni-Al boundaries and is defined as the (negative) slope of the curve of number of occurrences versus the size of boundary features on the micrographs. Thus, it returns the exponent of the power law connecting these two variables and its variation over dimensional scale. This indicates changes in the phenomena of the fabrication process producing the fractal microstructure of the material.

DSC measurements were performed on all samples using a Setaram Labsys DSC system. Samples of ~25 mg were cut from similar positions, where also the microstructural characterization was conducted (r ~3 mm). Subsequently, the measurements were performed in Al_2O_3 crucibles in argon atmosphere up to a temperature of 1773 K using a heating rate of 10 K/min. Laboratory XRD measurements were carried out on the as-deformed HPT samples, samples after DSC measurements and ignited samples using a Bruker-AXS D8 Advance diffractometer with Cu Kα radiation (λ = 1.5406 Å) at 40 kV voltage and 40 mA current. The

X-ray diffractograms were recorded using Bragg-Brentano geometry in a 2θ range from 20 to 90°, a 0.01° step width and a scan speed of 1.2 s per step. Phase identification and peak indexing was performed based on standard peak positions of the individual phases Ni [44], Ni_3Al [45], NiAl [46], Al_3Ni_2 [47], Al_3Ni [48] and Al [49] provided by the International Centre for Diffraction Data (ICDD). As detailed later, for the samples subjected to five and eight rotations, XRD revealed already noticeable amounts of the intermetallic Ni_3Al phase formed during the HPT process. To reveal the critical strain (i.e., radius and number of rotations) for mechanically induced Ni_3Al formation, these two samples were selected for lateral resolved scanning transmission synchrotron XRD measurements. Line scans across the sample radius were performed at the high energy materials science beamline P07 at DESY (Deutsches Elektronen-Synchrotron, Petra III, Hamburg, Germany) using a 0.5 × 0.5 mm² sized X-ray beam with an energy of 87 keV (λ = 0.14235 Å). Each sample was mounted with its former torsional axis parallel to the X-ray beam using a translation stage. Diffraction patterns were recorded at radial positions of R= 1, 2, 3 and 4 mm using a Perkin-Elmer 2D detector. Prior to the measurements, the setup was calibrated using a LaB_6 line position standard of SRM 660c type provided by the National Institute of Standards and Technology (NIST). Subsequently, the patterns were integrated along the azimuthal direction to observe corresponding diffractograms of the individual measurements, i.e. along the radial direction. Standard peak positions for Al, Ni and Ni_3Al were calculated and indexed using the lattice parameter of the individual phases provided by the ICDD cards of the respective phases specified above.

To directly monitor the self-propagating reaction and the subsequent intermetallic phase formation of the Ni-Al specimens during ignition, the sample deformed for 8 rotations was selected and analyzed in detail using *in situ* synchrotron X-ray measurements at sector 32-ID-B of the Advanced Photon Source (APS) at Argonne National Laboratory (ANL); the experimental set-up is shown in Fig. 2. The X-ray energy was 25.39 keV with a corresponding

wavelength of λ = 0.488 Å. The X-ray beam was focused down to 50 × 50 μm^2 along the edge of the thin cylindrical sample and the diffraction signal was imaged using a $Lu_3Al_5O_{12}$:Ce scintillator mounted Lavision HS-IRO image intensifier imaged with a Photron SA-Z high speed camera at 20 kHz in pre-trigger mode. The sample was mounted on a 3-axis stage and moved into position to get the glancing angle X-rays, since the beam is completely absorbed by the 0.8 mm thick sample. The sample distance from the scintillator was 290 mm at an angle of 10.15° degrees. The edge of the sample, where the diffracted beam is collected, was supported by an amorphous soda lime glass slide to prevent sample movement without producing a diffraction pattern. The sample was ignited using a resistively heated tungsten coil that was placed in contact at the top of the sample supporting it on its edge. The sample was simultaneously imaged using a FLIR SC2500 near-infrared camera operated at 1000 Hz and a commercial CCTV camera that were both operated remotely. When the reaction was observed on the CCTV video stream relayed to a monitor at the control room, all the cameras were manually triggered to record the last 2 s of the event. The resulting diffraction patterns were analyzed using the HiSPoD software developed by ANL and calibrated using Al foils. The Debye-Scherrer rings were integrated over a Phi angle (azimuthal direction) range between 150-210°. Standard peak positions for Al_3Ni, Al_3Ni_2 and NiAl were calculated and indexed using the lattice parameter of the individual phases provided by the ICDD cards of the respective phases specified above [44–49].

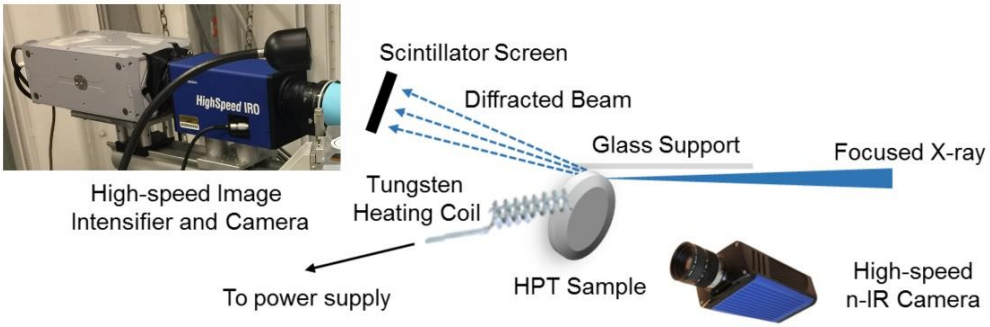

Fig. 2. Schematics showing the *in situ* synchrotron X-ray diffraction setup.

3. Results and Discussion

3.1 Microstructure and phase evolution during HPT deformation

Fig. 3 shows representative SEM micrographs of the Ni-Al samples deformed to different numbers of rotations. As expected, higher strain levels ensure full densification accompanied by substantial refinement of the powder particles. Up to two rotations, corresponding to an equivalent strain of about 27 at r = 3 mm, a significant amount of residual porosity can be observed. These pores most likely stem from a loss of improperly bonded powder particles during metallographic sample preparation and not from a low sample density itself. For this reason, the just compressed specimens (zero rotations) were also excluded from the SEM analysis. However, Fig. 3 shows that at least two rotations at room temperature are needed to ensure pore free bonding of the powder particles. While the dimensions of the individual phases are still up to the micrometer range after two rotations, already significant grain refinement occurs. After five and eight rotations, nanolamellar structures with dimensions significantly below 100 nm are obtained. While for up to five rotations the lamellar structure refines and aligns preferentially along the shear direction, i.e. parallel to the tangential direction, especially the structure after eight rotations looks different. At this strain level, many lamellae are rotated with respect to the shear plane. The image taken at higher magnification reveals that individual lamellae are displaced and seem to be sheared off. Such features can be frequently found in case of strain localization during severe deformation of composites [20,50–52]. These locally enhanced shear strains do not only promote locally enhanced refinement, but eventually also result in chemical intermixing or intermetallic phase formation, i.e. features that are not desirable for self-reactive specimens.

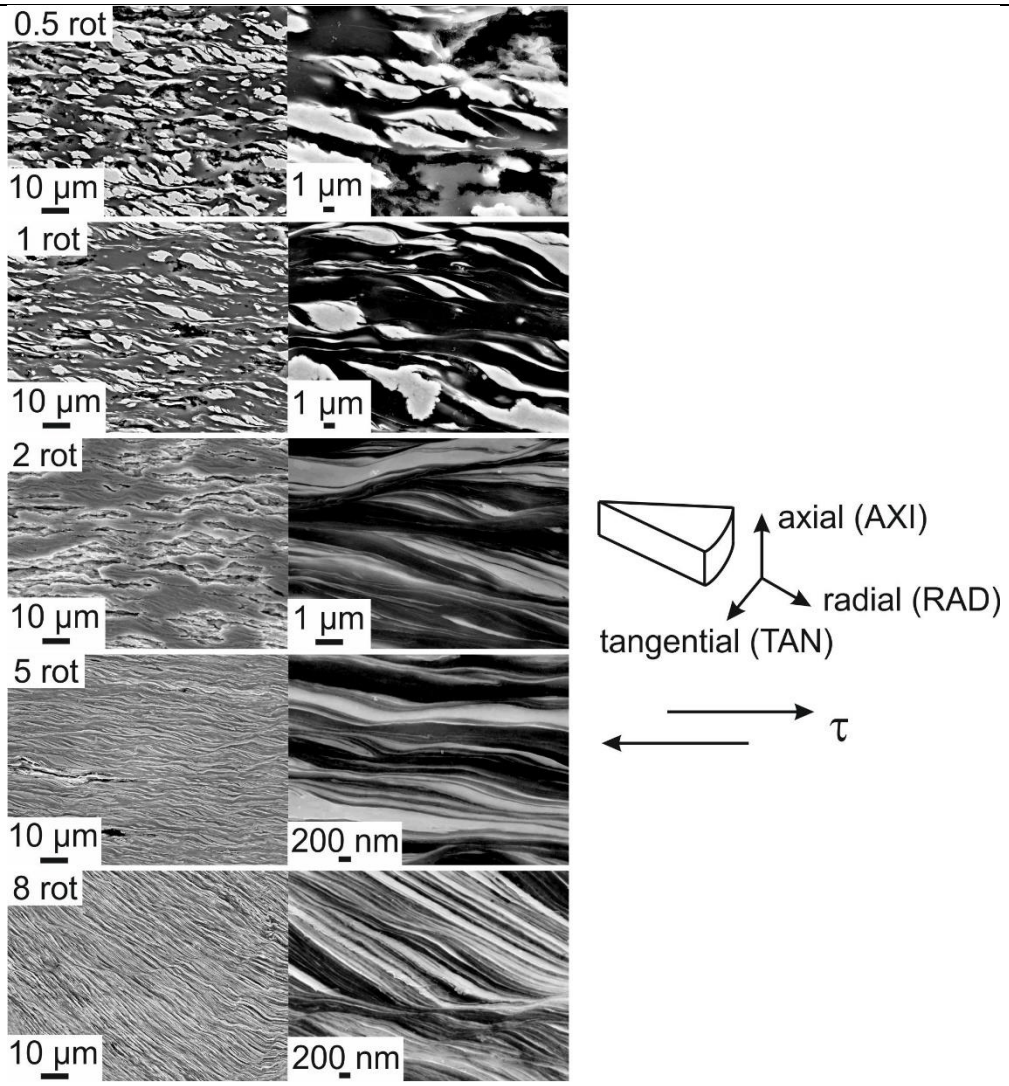

Fig. 3. Representative microstructures of the Ni-Al samples subjected to HPT for different numbers of rotation. All images were taken in radial direction at *r* ~3 mm.

Fig. 4 illustrates the dependence of the fractal dimension in the SEM micrographs on magnification scale (in kx, i.e., 1000 times magnification) for samples subjected to 0.5, 1, 2, 5 and 8 rotations. While a fractal dimension of two describes smooth interfaces, higher values indicate more complicated interfacial structures along with increased interfacial area. It thus provides a quick estimation of a, beside the lamellae spacing, potentially important parameter that can affect the reaction kinetics. As expected, the fractal dimension initially decreases with feature scale because of the typical log-normal size distribution of the starting Ni and Al powders, but stabilizes at higher magnifications due to the submicron geometrical roughness of

the powder granules. With increasing number of rotations, the fractal dimension at a fixed scale initially decreases due to intergranular friction and local deformation of the boundaries, thus eliminating finer geometric features, resulting in micro-bonding of the grains into combined, larger blob aggregates. Upon further straining, however, the fractal dimension generally rebounds again to higher values across scale because new feature complexity is generated during deformation. This stems from the extensive shear deformation of the individual phases into alternating finer lamellae of progressively smaller thickness, as well as 'Swiss roll-up' curls of the lamellar structures at local flow instabilities. While homogenous plastic flow is present at the beginning, it is presumably countered by the increasing confinement and strain hardening of the two phases accompanied by formation of intermetallics, resulting in strain localization and according rotation of the lamellae with respect to the shear direction. The geometrical features of the generated new boundaries thus contribute to raising the fractal dimension during the process. These phenomena are congruent and comparable with those observed in Ni and Al powder consolidates prepared by other severe plastic deformation methods such as HEBM but as well with HPT deformation of other composite materials [16–23,26,52,53].

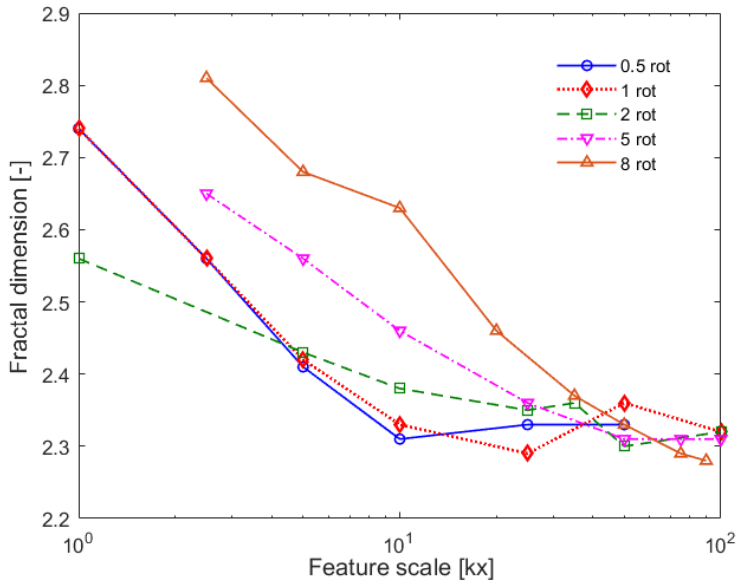

Fig. 4. Variation of fractal dimension on SEM micrographs taken at r ~3 mm with feature scale during HPT processing.

Laboratory XRD measurements were conducted to reveal if apart from Ni and Al any intermetallic phase(s) formed during HPT processing. The results are presented in Fig. 5, reflecting the microstructural observations. With increasing strain (i.e., number of HPT rotations), the Al and Ni peaks broaden due to substantial microstructural refinement. In addition, for the samples deformed up to five and eight rotations, reflections of the Ni_3Al phase are present. Phase formation was frequently observed during severe plastic deformation and related to the large defect densities created. As the resulting phases often correspond to the equilibrium phases present at elevated temperatures, the concept of an effective processing temperature, T_{eff}, has been introduced [54,55]. Based on this concept, T_{eff} should be larger than about 1400 K here, because above this temperature only Ni_3Al and NiAl exist. Nevertheless, the NiAl phase was not detected in any of the as-deformed samples, but only the Ni_3Al phase. While certainly further investigations are required, the conflict with the concept of an effective temperature might be explained based on the underlying processes of mechanical intermixing. As the mechanically induced chemical intermixing, necessary to induce formation of the intermetallic Ni_3Al phase is mainly governed by the deformation of the individual phases and the defects created within them (e.g. roughening of the interfaces, size of the phases, etc.) [51,56], it is not unreasonable that deviations from the concept of an effective temperature occur. However, the mechanically induced phase formation at comparably low strains is in good agreement with earlier findings in the Ni-Al system, although presumably due to the elevated HPT processing temperatures (573 K) and different chemistry (50 at.% Al) Al_3Ni formed [34].

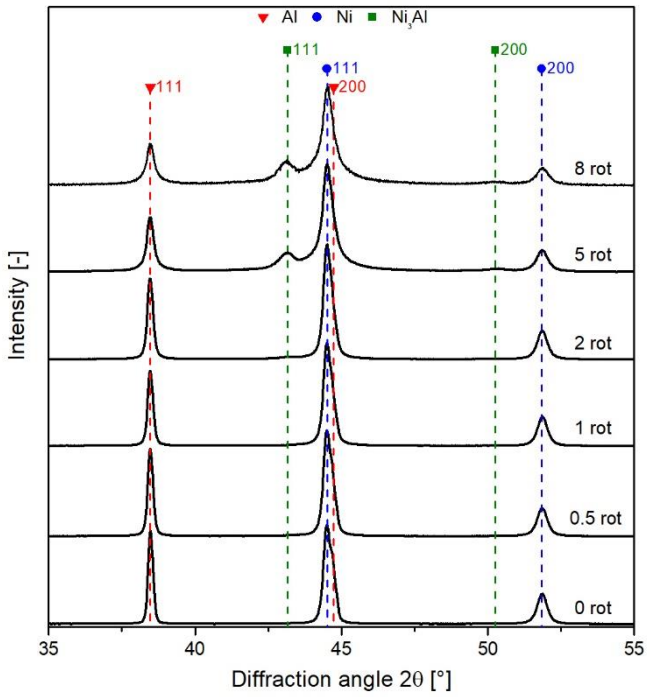

Fig. 5. Laboratory X-ray diffractograms of the Ni-Al samples consolidated and HPT deformed to different number of rotations.

To reveal the critical strains for deformation induced intermetallic phase formation, position resolved scanning transmission synchrotron measurements were performed on those samples giving Ni_3Al reflections in the laboratory equipment (i.e., with five and eight rotations) and the results are presented in Fig. 6. Four positions were analyzed for each of those samples, moving in 1 mm steps from the center towards the edge of the sample in radial direction. The measurement positions at r = 1, 2, 3 and 4 mm are denoted in Fig. 6 as $R_{1\ mm}$, $R_{2\ mm}$, $R_{3\ mm}$ and $R_{4\ mm}$, respectively. As expected, both samples show reflections of the intermetallic Ni_3Al phase, however, only for larger radii, indicating that a certain amount of strain is necessary for its formation. This is in line with the microstructural observations, where for both, five and eight rotations, nanoscale features presumably required for intermixing can be found. No Ni_3Al peaks are present in the sample deformed for five rotations at r < 3 mm. As the samples subjected to five rotations seem to deform homogenously (Fig. 3), a critical strain for the phase

formation of $\varepsilon_{vM} \sim 68$ can be estimated from Eq. 1. For both samples, the intensity of the Ni_3Al peaks increases with strain, i.e. when moving towards the edge of the HPT disk. Thus, for a given radius higher intensities should be present in the eight rotation sample compared to the one subjected to only five rotations. However, this only holds true for the largest radius, while for $r < 4$ mm the intensities of Ni_3Al remain at a rather constant level. Presumably this discrepancy is caused by the occurrence of strain localization at higher strain levels (compare Fig. 3), complicating a direct comparison between the specimens. Nevertheless, the results clearly emphasize that Ni_3Al formation can already occur at low number of rotations.

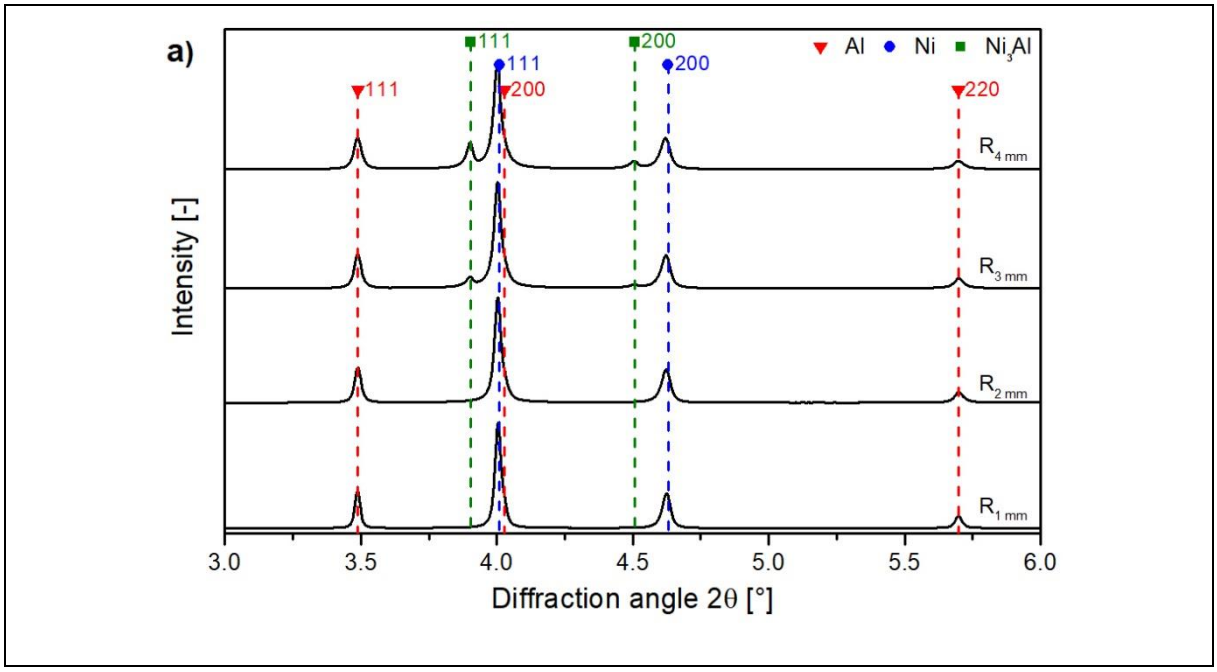

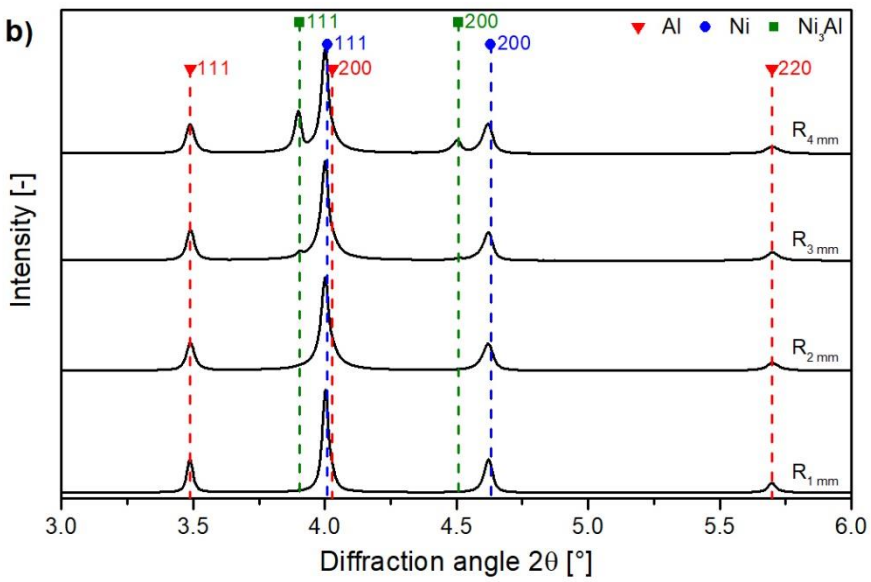

Fig. 6. Radial phase evolution of the Ni-Al samples subjected to HPT for a) five and b) eight rotations. Radial positions are denoted as R_x, where x is the distance in mm.

3.2 Thermal analysis and phase formation at low heating rates

In general, thermomechanically induced phase formation should be avoided as it could deteriorate the ignition and reaction behavior of self-reactive samples. However, the phase fractions formed may not be sufficiently large to subdue the targeted reactions. To elucidate the influence of pre-existing intermetallic phases as well as the phase spacing of the Ni-Al nanocomposite on the ignition behavior, DSC measurements were performed on all samples and the results are shown in Fig. 7a. Independent of the applied strain and, thus, phase spacing and phase morphology, exothermic reactions occur well below the melting point of pure aluminum (933 K). This also holds true for the just compressed powder blends, but may not be surprising, as also for these specimens a considerable amount of strain ($\varepsilon \sim 1$) was already applied. Such strains seem to be sufficient to decrease the phase dimensions, fracture the native oxide layer and enhance the interfacial area, all of them facilitating the occurring reactions. However, with increasing number of rotations, i.e. structure refinement, the onset temperature of the exothermic reaction is progressively shifted towards lower temperatures. While for the

as-compacted powder blends the reaction proceeds at about 750 K, it already starts at about 450 K after eight rotations. This is in line with earlier observations on sputtered or ball milled Ni-Al samples, where reduced phase dimensions accelerate the reaction kinetics (e.g. compare Refs. [15,16,18,20]). These exothermic reactions are indicative of intermetallic phase formation. With decreasing microstructural dimensions, the exothermic peaks tend to broaden and the overall heat release somewhat diminishes. While the broadening might be attributed to the size distributions of the HPT deformed microstructures and their respective onset temperatures, the diminishing exothermal heat flow is most likely a consequence of the formation of intermixed regions or mechanically formed compounds that reduce the available enthalpy that can be released in the form of heat. Intermixed interfacial layers have not only been observed in Ni-Al samples produced by means of plastic deformation [57], but also for sputtered multilayers having small sublayer dimensions (i.e., 12.5 nm), with similar effects on the released heat as found here for the HPT samples [58]. Furthermore, the exothermic reaction seems to propagate in two stages beyond 2 rotations, which becomes evident for the samples deformed to higher strains, where two peaks can be clearly identified, compare Fig. 7a. However, also for the just compressed powder blends the distinct shoulder of the exothermic peak indicates a reaction occurring in two stages. Two distinct peaks in DSC analysis of self-reactive nanocomposites have been observed earlier and were attributed to isolated nucleation and growth of the intermetallic phases, in some cases coupled to the formation of an amorphous precursor phase [59,60]. Although the applied strain clearly shifts the onset temperatures (Fig. 7a), similar reaction sequences seem to occur for all specimens. The measured heat flow over the whole investigated temperature range is exemplarily plotted for the sample deformed for five rotations in Fig. 7b. For all specimens, the exothermic reactions are completed at 900 K at maximum and for higher temperatures two distinct endothermic peaks can be identified for all samples. The first occurs at about 1150 K, while the other proceeds at 1425 K. Both temperatures are in good agreement with the two peritectic reactions expected from the Ni-Al

phase diagram [61] for the given composition. According to this phase diagram, Al_3Ni transforms at 1129 K into Al_3Ni_2 and liquid phase, while at 1411 K Al_3Ni_2 further decomposes into liquid phase and NiAl. At ~1560 K another exothermic peak can be identified. The origin of this peak at ~1560 K (Fig. 7b) could not unambiguously clarified, but might stem from possible reactions of the sample with the alumina crucible. If kinetically permitted these reaction sequences inversely occur upon cooling and NiAl reacts to Al_3Ni_2 and remaining liquid phase, while at even lower temperature additionally Al_3Ni forms. Based on these reactions it can be assumed that after the exothermic reactions Al_3Ni, Al_3Ni_2 and remaining Al or Ni should be present.

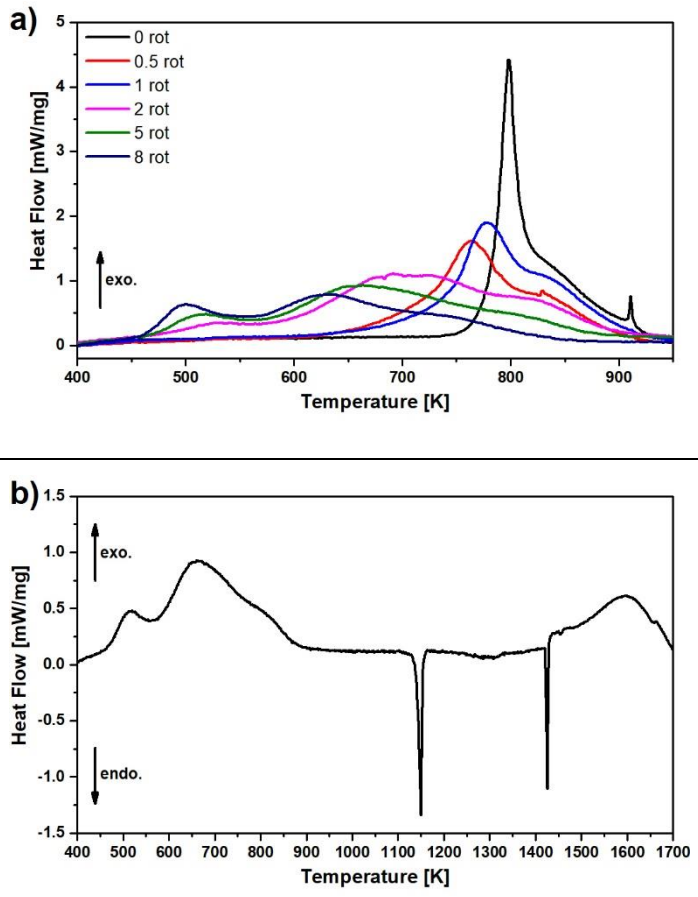

Fig. 7. a) Heat flow of the exothermic reactions occurring in the specimens subjected to different strains by HPT as revealed by DSC in Ar atmosphere at a heating rate of 10 K min^{-1}; b) Measured heat flow in the whole temperature range (up to 1773 K) exemplarily shown for the sample deformed for five rotations.

The reacted DSC samples were subsequently crushed, ground into powders and analyzed in the lab XRD to identify the formed phases. The resulting diffractograms of all specimens are presented in Fig. 8. As can be noticed, in agreement with the DSC measurements, the final phase composition of the samples does not differ significantly. Apart from a minor amount of Al, all samples consisted predominantly of the Al_3Ni and Al_3Ni_2 phases, as expected for the given chemical composition. Only in case of the samples deformed to the highest number of rotations a minor fraction of the equimolar NiAl phase was found. The traces of Ni_3Al that were found in the samples deformed for five and eight rotations were not detected anymore after the DSC runs. Thus, it can be concluded that the reaction kinetics are subject to change if the starting phase dimensions are reduced, but not the reaction sequence itself.

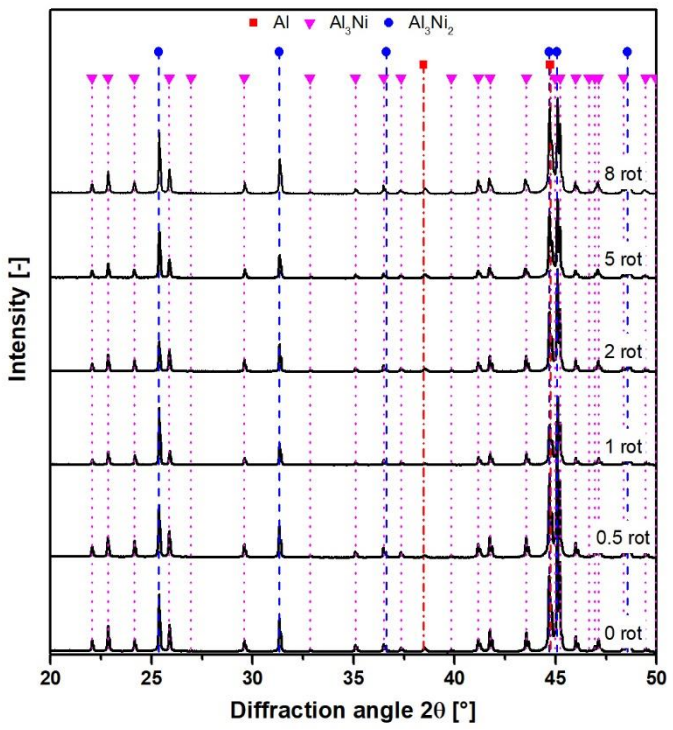

Fig. 8. Diffractograms of the DSC samples revealing the final phase compositions. Independent of the applied strain during HPT, the samples finally consist of Al_3Ni and Al_3Ni_2 with some minor fractions of Al.

3.3 Reaction sequence and phase evolution during ignition

As the heating rate is known to potentially influence the reaction sequence and final phase composition [13,41], the results obtained on the DSC samples at rather low heating rates may not be representative for self-propagating reactions occurring in ignited samples. Therefore, another set of all samples was ignited and analyzed post mortem in the lab XRD. In addition, to monitor the occurring reactions, one sample was analyzed in an *in situ* synchrotron experiment accompanied by a highspeed near-infrared camera. For this experiment, the sample deformed for eight rotations was chosen. This sample was selected as it already contains a fraction of Ni_3Al. Thus, it allows conclusions about whether the structural gradient along the disk radius or the mechanically induced intermetallic phase formation prevent ignition or reaction throughout the whole HPT disk.

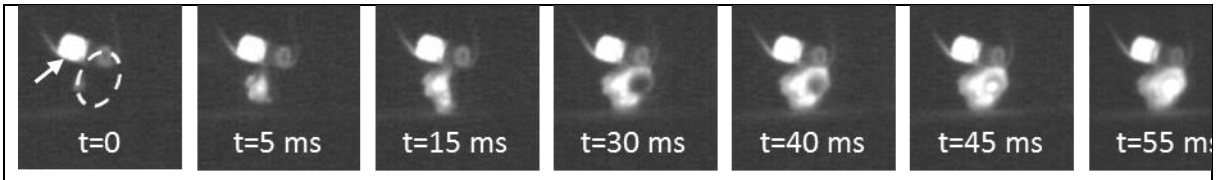

Fig. 9. Image series from high-speed near-infrared imaging at 1000 Hz showing the propagation of the reaction in the sample deformed for eight rotations. It can be noticed that the reaction first propagates at the edge of the sample before travelling towards the center that initially appears dark. The sample is outlined with dashed lines in the first frame, with the bright object marked with an arrow in the top left corner being the hot tungsten coil to ignite the sample.

The image series from high-speed near-infrared imaging are shown in Fig. 9. The contact point between the bright tungsten heating coil and the HPT disk appears darker due to heat conduction to the sample, reducing the temperature locally. Given times are relative to the first sign of a reaction within the sample (i.e., t=0 for the first frame). The reaction starts at a location on the outer edge of the sample away from the contact point with the heating coil and propagates along the outer edge. After forming a complete ring, the reaction front slowly propagates radially

towards the center. Following an incubation period of about 10 ms, a hot spot appears at the center and reacts further for another 10 ms. The reactions are completed after this stage. The morphology of the propagation front can be expected from the nature of the HPT disk, with the applied shear strain linearly increasing in radial direction from the disk center. As the periphery of the disk undergoes higher strains, these areas are refined to a higher degree compared to the center. Due to the reduced diffusion paths these regions can react faster, whereas the reaction kinetics towards the center slows down. Nevertheless, despite this structural gradient the disk fully reacts. Based on the simultaneously recorded diffraction data from the right edge of the HPT sample, the occurring reaction sequences after preheating with the tungsten coil can be determined, compare the obtained diffraction data in Figs. 10 - 13. Fig. 10 shows the integrated diffraction patterns as a function of relative time (y-axis). It has to be noted that the timescale of the diffraction experiment was not synchronized with the near-infrared image series and thus a direct comparison of the relative times of both experiments is not possible. The initial peaks between 2θ = 12 - 16° can be assigned to Al and Ni. There is also another weak peak at around 7.5° possibly stemming from Al_3Ni, that already formed upon pre-heating the sample with the tungsten coil. No distinct peaks of the Ni_3Al phase could be detected, as opposed to the already reported laboratory and synchrotron XRD analysis (Figs. 5 and 6), although they might exist in relatively small amounts. This might be a consequence of the small phase fraction and probing the sample locally (~50 µm) in this *in situ* experiment. The reaction front passes across the small area of interest at a relative time of ~160 ms. At that stage, the initial constituents Al and Ni along with the already formed Al_3Ni rapidly react to Al_3Ni and Al_3Ni_2, compare Fig. 11. The patterns at this stage are nearly continuous, indicating the formation of very fine crystallites with random orientation. After a period of around 30 ms, the second stage commences to produce Al_3Ni_2 with a significant amount of melt fraction, which is in agreement with the Ni-Al phase diagram for the given composition, as soon as temperatures above ~1129 K are reached. A slight shift of the recorded pattern to lower 2θ angles with respect to the indicated

room temperature standard peak positions can be assigned to the inherent thermal expansion of the respective phases.

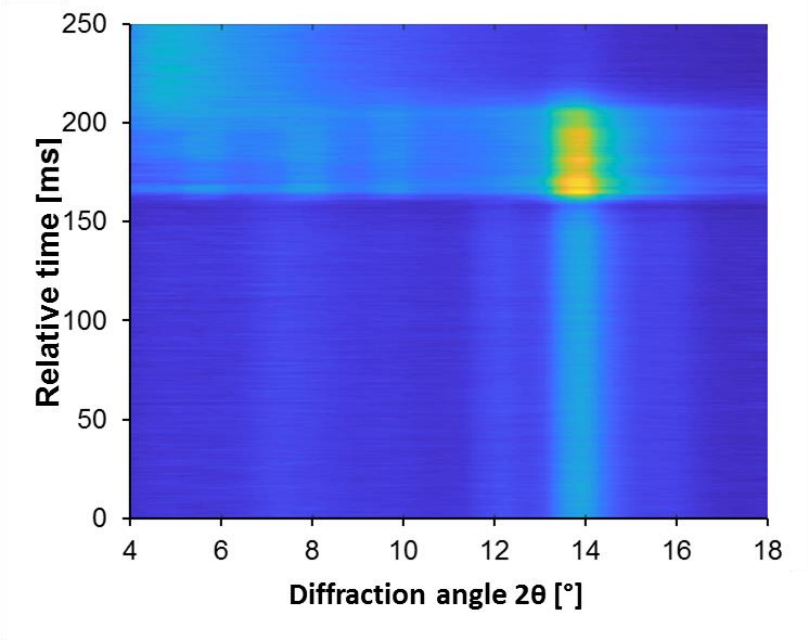

Fig. 10. Time series of integrated diffraction patterns obtained during the reaction of a Ni-Al sample deformed for eight rotations. The reaction front passes across the measurement spot at a relative time of ~160 ms.

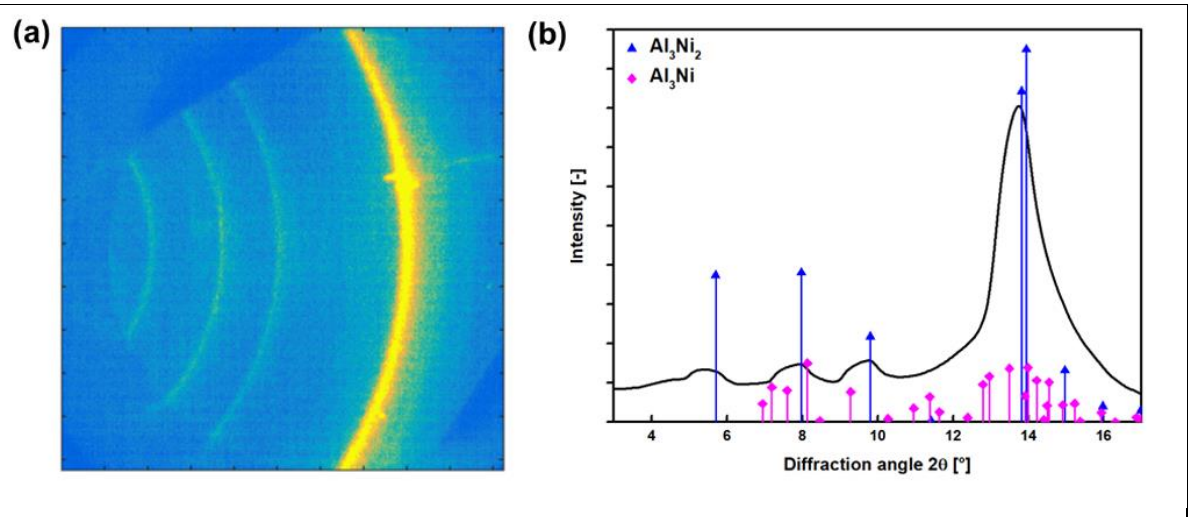

Fig. 11. a) The diffraction pattern of the sample deformed for eight rotations at a relative time of ~165 ms (time averaged over 5 ms) shows Debye-Scherrer rings from Al_3Ni and Al_3Ni_2 and b) the corresponding integrated pattern with according room temperature standard peak positions for Al_3Ni_2 andAl_3Ni. Due to the small area probed, the continuous Debye-Scherrer rings suggest the formation of fine and randomly oriented crystallites.

Almost all peaks disappear at a relative time of ~200 ms and only a broad halo at around 2θ ~5° remains, as shown in Fig. 12, at a relative time of 225 ms. The diffraction patterns from this time on show a single weak diffraction spot originating from NiAl. This might be due to almost complete melting of the product phases Al_3Ni_2 and Al_3Ni at this sample state which leaves, according to the Ni-Al phase diagram, NiAl as the only solid phase if the peritectic line at ~1411 K is exceeded, and the temperatures applied do not exceed the melting point of NiAl. Again a slight shift of present peak in the recorded pattern to lower 2θ angles with respect to the indicated room temperature standard peak position is observed which can be related to the thermal expansion of the NiAl phase at elevated temperature. The two spots clearly observed in Figs. 11 and 12 and partially in Fig. 13 at the diffraction angle of ~13.5° at approximately two o'clock direction do not originate from the sample, but rather from an object in the path of the beam, either part of the aluminum mount used to secure the sample or the tungsten coil. This was evident as these spots were not affected by the transformations in the sample and were present before and after the reactions.

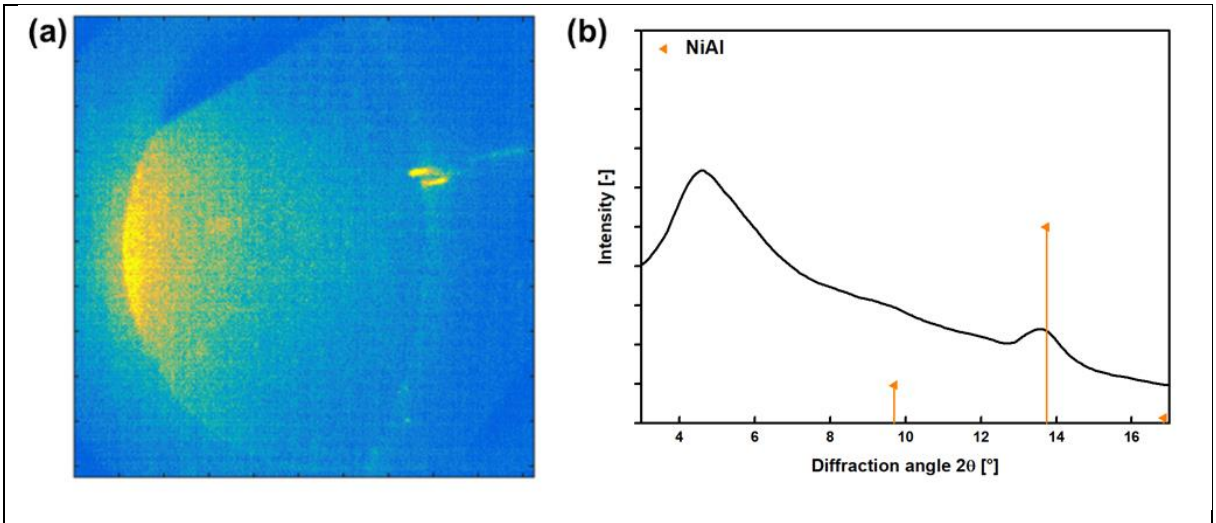

Fig. 12. a) The diffraction pattern of the sample deformed for eight rotations at a relative time of ~225 ms (time averaged over 5 ms) shows a broad halo with a weak diffraction spot from NiAl and b) the corresponding integrated pattern with the calculated room temperature standard peak positions for NiAl.

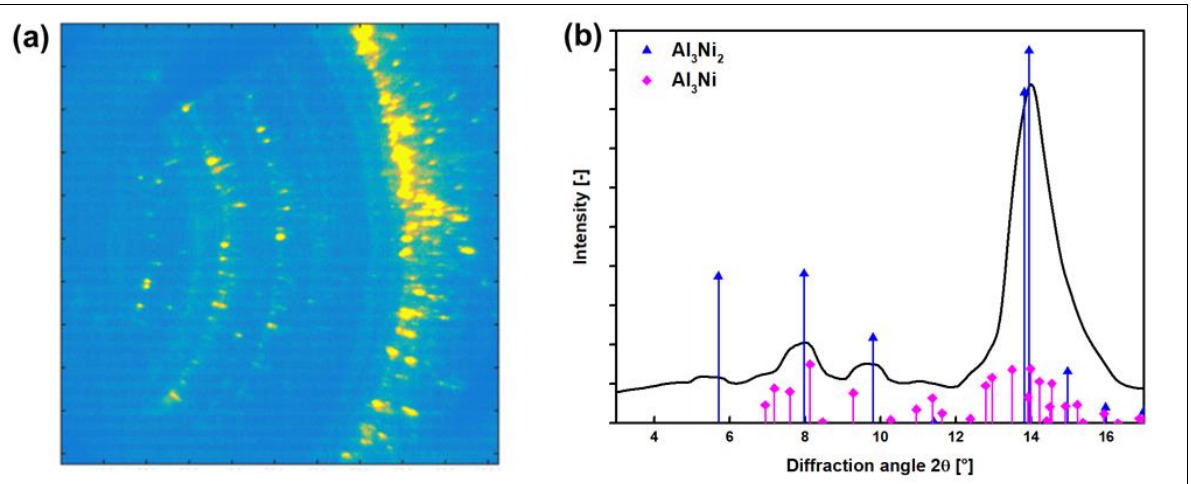

Fig. 13. a) The diffraction pattern (averaged over 100 frames) after the reaction of the sample deformed for eight rotations shows multiple diffraction spots originating from Al_3Ni_2 and Al_3Ni and b) the corresponding integrated pattern with calculated room temperature standard peak positions of Al_3Ni_2 and Al_3Ni.

The diffraction peaks from the cooled sample after reaction are shown in Fig. 13. After the reactions are fully completed, peaks from Al_3Ni_2 and Al_3Ni are observed, which should have formed again during solidification and cooling, being again in good agreement with the Ni-Al phase diagram and also with the results obtained at low heating rates (i.e., the DSC experiments). At this stage, the recorded peaks in the pattern fit very well to the indicated room temperature standard peak positions due to the lack of a mismatch caused by the thermal expansion of the respective phases. Such kind of multi-stage reactions have also been observed in reacting green compacts fabricated from HEBM Ni-Al powders using two-color near-infrared imaging [23]. The reactions seem to stagger at the peritectic temperature of 1411 K as Ni_2Al_3 dissociates into melt and NiAl endothermically, when the self-heating rates are not sufficient to rapidly overcome this. Likewise, melting of any remaining Ni can also stagger the reactions due to its endothermic melting at 1728 K, although this has not been observed in the HPT samples.

To elucidate the effect of the phase spacing and morphology on the phase constitution after ignition, the various HPT samples after ignition were also analyzed in the lab XRD. The obtained diffractograms are shown in Fig. 14. Independent of the sample, Al_3Ni and Al_3Ni_2 are present as final phases. In addition, for the samples subjected to less than two rotations, a minor amount of Al can be detected as well. This might be a consequence of the still relatively large phase dimensions in case of these samples, resulting in longer diffusion distances and accordingly retarded reaction kinetics.

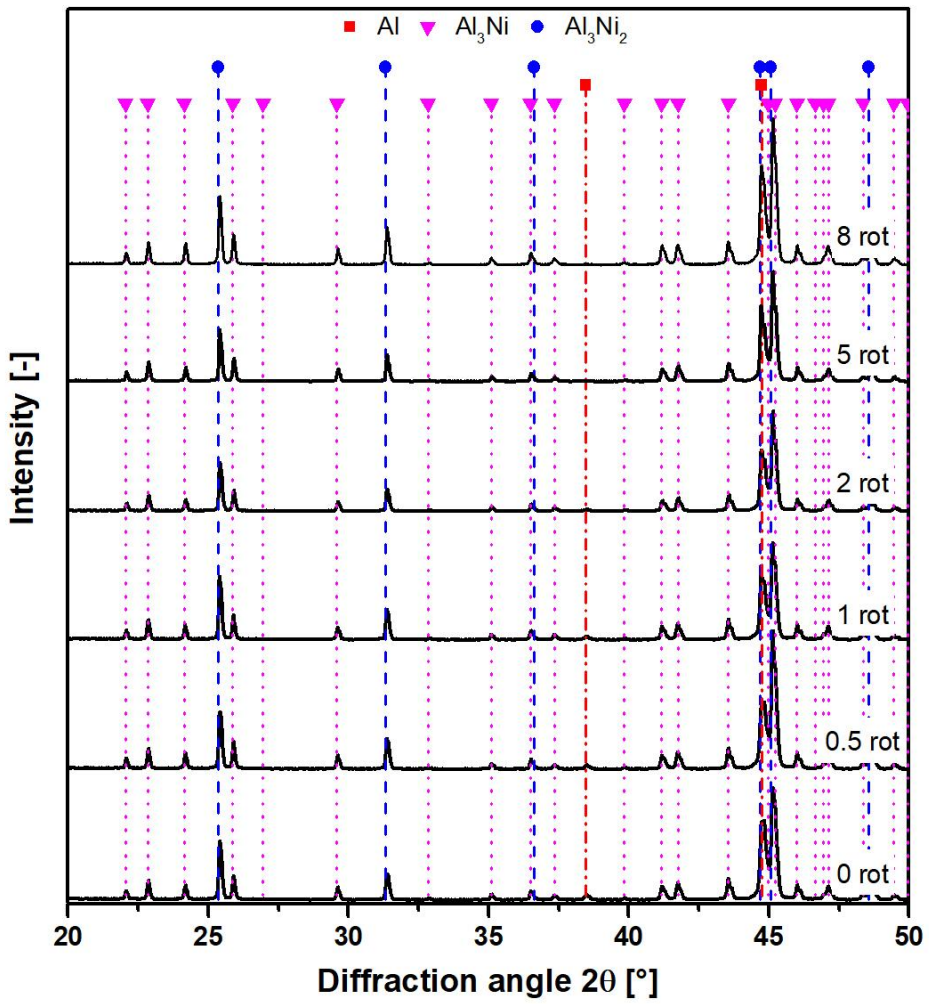

Fig. 14. X-ray diffractograms of the ignited and fully reacted HPT samples deformed to different strain levels.

Comparing the different heating rates, i.e. low during DSC and high during the ignition experiments, the product phases do not differ significantly (Fig. 8). Hence, for the HPT samples studied herein, the heating rate does not seem to cause significant differences with respect to

the reaction sequence. This widely holds true also for the applied strain, although the samples deformed to higher numbers of rotations react completely, while for the just compressed or slightly deformed disks some aluminum remains. Presumably this difference is caused by the enhanced defect densities and shorter diffusion pathways. Based on the experiments and the known asymmetric diffusivity in the Ni-Al system [62,63], it is obvious that the reaction starts with the interdiffusion of Ni into Al, resulting in the formation of Al_3Ni. This results not only in a heat release due to the phase formation, but presumably also enhances the diffusivity in the Ni phase due to the increasing vacancy concentration. As a consequence, Al_3Ni_2 can form and in case that sufficient heat is either released by the self-propagating reaction or from a heating source (i.e., such as in case of the DSC), it can dissociate at elevated temperatures into a liquid phase and the equimolar NiAl phase. Thus, based on the *in situ* diffraction data and the investigated composition, the maximum reaction temperatures can be expected to be above 1411 K, but below the melting point of NiAl (1924 K).

4. Summary and Conclusions

In the present study, a first attempt to synthesize bulk self-reactive Ni-Al samples by high pressure torsion (HPT) at ambient temperature was performed. Detailed investigations of samples deformed to different strains and thus varying structural dimensions clearly show that HPT is capable to produce reactive specimens on a bulk scale. Despite the structural gradient along the disk radius, the samples with a composition of 70 at.% Al deformed by HPT are highly reactive and can be ignited significantly below the Al melting point, yielding a product predominantly consisting of Al_3Ni_2 and Al_3Ni and minor fractions of NiAl, while reaching reaction temperatures significantly above 1400 K. While the applied increasing strains cause a significant refinement and lower the onset temperatures of the reaction, diffraction analysis revealed mechanically induced intermetallic phase (Ni_3Al) formation at higher strains. Avoiding intermetallic phase formation while refining the structure even further could certainly

improve the ignition and reaction behavior. Intermetallic phase formation could occur by mechanical intermixing, which could be accelerated by strain localization (favored at low temperatures) but also thermally induced. Ideal processing conditions yielding maximum refinement without intermetallic phase formation are thus hard to predict and inspection of samples processed by HPT at different temperatures is required to understand the predominant formation processes and to optimize synthesis conditions.

Acknowledgments

The authors gratefully acknowledge the financial support under the scope of the COMET program within the K2 Center “Integrated Computational Material, Process and Product Engineering (IC-MPPE)” (Project No 859480). This program is supported by the Austrian Federal Ministries for Transport, Innovation and Technology (BMVIT) and for Digital and Economic Affairs (BMDW), represented by the Austrian research funding association (FFG), and the federal states of Styria, Upper Austria and Tyrol. This work was further supported by the Department of Energy National Nuclear Security Administration under Award Number DENA0002377. Additional support was provided through the ERC Advanced Grant INTELHYB (grant ERC-2013-ADG-340025). This research used resources of the Advanced Photon Source, a U.S. Department of Energy (DOE) Office of Science User Facility operated for the DOE Office of Science by Argonne National Laboratory under contract number DE-AC02-06CH11357. The authors would also like to acknowledge the assistance of Alex Deriy and Matthew Beason.

References

[1] A.G. Merzhanov, ed., 40 YEARS OF SHS: A LUCKY STAR OF A SCIENTIFIC DISCOVERY A Presentation with Elements of a Scientific Lecture, 2012th ed., Bentham Science Publisher, Brussel, Belgium, 2012. doi:10.2174/97816080512811120101.

[2] U. Anselmi-Tamburini, Z.A. Munir, The propagation of a solid-state combustion wave in Ni-Al foils, J. Appl. Phys. 66 (1989) 5039–5045. doi:10.1063/1.343777.

[3] R. Armstrong, Theoretical models for the combustion of alloyable materials, Metall. Trans. A. 23 (1992) 2339–2347. doi:10.1007/BF02658035.

[4] T.S. Dyer, Z.A. Munir, V. Ruth, The combustion synthesis of multilayer NiAl systems, Scr. Metall. Mater. 30 (1994) 1281–1286. doi:10.1016/0956-716X(94)90259-3.

[5] A. Varma, A.S. Rogachev, A.S. Mukasyan, S. Hwang, Combustion Synthesis of Advanced Materials: Principles and Applications, Adv. Chem. Eng. 24 (1998) 79–226. doi:10.1016/S0065-2377(08)60093-9.

[6] K. Morsi, Review: Reaction synthesis processing of Ni-Al intermetallic materials, Mater. Sci. Eng. A. 299 (2001) 1–15. doi:10.1016/S0921-5093(00)01407-6.

[7] P. Zhu, J.C.M. Li, C.T. Liu, Adiabatic temperature of combustion synthesis of Al-Ni systems, Mater. Sci. Eng. A. 357 (2003) 248–257. doi:10.1016/S0921-5093(03)00249-1.

[8] D. Tingaud, L. Stuppfler, S. Paris, D. Vrel, F. Bernard, C. Penot, F. Nardou, Time-resolved X-ray diffraction study of SHS-produced NiAl and NiAl-ZrO2 composites, Int. J. Self-Propagating High-Temperature Synth. 16 (2007) 12–17. doi:10.3103/s1061386207010025.

[9] A.S. Rogachev, S.G. Vadchenko, A.A. Nepapushev, S.A. Rogachev, Y.B. Scheck, A.S. Mukasyan, Gasless Reactive Compositions for Materials Joining: An Overview, Adv. Eng. Mater. 20 (2018) 1701044. doi:10.1002/adem.201701044.

[10] F. Baras, V. Turlo, O. Politano, S.G. Vadchenko, A.S. Rogachev, A.S. Mukasyan, SHS in Ni/Al Nanofoils: A Review of Experiments and Molecular Dynamics Simulations, Adv. Eng. Mater. 20 (2018) 1800091. doi:10.1002/adem.201800091.

[11] K.J. Blobaum, D. Van Heerden, A.J. Gavens, T.P. Weihs, Al/Ni formation reactions: Characterization of the metastable Al9Ni2 phase and analysis of its formation, Acta Mater. 51 (2003) 3871–3884. doi:10.1016/S1359-6454(03)00211-8.

[12] H. Nathani, J. Wang, T.P. Weihs, Long-term stability of nanostructured systems with negative heats of mixing, J. Appl. Phys. 101 (2007) 104315. doi:10.1063/1.2736937.

[13] J.C. Trenkle, L.J. Koerner, M.W. Tate, S.M. Gruner, T.P. Weihs, T.C. Hufnagel, Phase transformations during rapid heating of Al/Ni multilayer foils, Appl. Phys. Lett. 93 (2008) 81903. doi:10.1063/1.2975830.

[14] D.P. Adams, Reactive multilayers fabricated by vapor deposition: A critical review, Thin Solid Films. 576 (2015) 98–128. doi:10.1016/j.tsf.2014.09.042.

[15] T.S. Dyer, Z.A. Munir, The synthesis of nickel aluminides by multilayer self-propagating combustion, Metall. Mater. Trans. B. 26 (1995) 603–610. doi:10.1007/BF02653881.

[16] D.Y. Kovalev, N.A. Kochetov, V.I. Ponomarev, A.S. Mukasyan, Effect of mechanical activation on thermal explosion in Ni-Al mixtures, Int. J. Self-Propagating High-Temperature Synth. 19 (2010) 120–125. doi:10.3103/s106138621002007x.

[17] K. V. Manukyan, B.A. Mason, L.J. Groven, Y.C. Lin, M. Cherukara, S.F. Son, A. Strachan, A.S. Mukasyan, Tailored reactivity of Ni+Al nanocomposites:

Microstructural correlations, J. Phys. Chem. C. 116 (2012) 21027–21038. doi:10.1021/jp303407e.

[18] A.S. Rogachev, N.F. Shkodich, S.G. Vadchenko, F. Baras, D.Y. Kovalev, S. Rouvimov, A.A. Nepapushev, A.S. Mukasyan, Influence of the high energy ball milling on structure and reactivity of the Ni + Al powder mixture, J. Alloys Compd. 577 (2013) 600–605. doi:10.1016/j.jallcom.2013.06.114.

[19] I.E. Gunduz, A. Kyriakou, N. Vlachos, T. Kyratsi, C.C. Doumanidis, S. Son, C. Rebholz, Spark ignitable Ni-Al ball-milled powders for bonding applications, Surf. Coatings Technol. 260 (2014) 396–400. doi:10.1016/j.surfcoat.2014.06.068.

[20] A. Hadjiafxenti, I.E. Gunduz, C.C. Doumanidis, C. Rebholz, Spark ignitable ball milled powders of Al and Ni at NiAl composition, Vacuum. 101 (2014) 275–278. doi:10.1016/j.vacuum.2013.09.006.

[21] C. Rebholz, I.E. Gunduz, T. Ando, C.C. Doumanidis, Miniature thermal matches: From nanoheaters to reactive fractals, Mater. Res. Express. 2 (2015) 45009. doi:10.1088/2053-1591/2/4/045009.

[22] B.A. Mason, T.R. Sippel, L.J. Groven, I.E. Gunduz, S.F. Son, Combustion of mechanically activated Ni/Al reactive composites with microstructural refinement tailored using two-step milling, Intermetallics. 66 (2015) 88–95. doi:10.1016/j.intermet.2015.06.009.

[23] A. Justice, I.E. Gunduz, S.F. Son, Microscopic two-color infrared imaging of Ni[sbnd]Al reactive particles and pellets, Thin Solid Films. 620 (2016) 48–53. doi:10.1016/j.tsf.2016.07.090.

[24] A. Hadjiafxenti, I.E. Gunduz, C. Tsotsos, T. Kyratsi, C.C. Doumanidis, C. Rebholz, Synthesis of reactive Al/Ni structures by ball milling, Intermetallics. 18 (2010) 2219–2223. doi:10.1016/j.intermet.2010.07.009.

[25] A. Hadjiafxenti, I.E. Gunduz, C. Tsotsos, T. Kyratsi, S.M. Aouadi, C.C. Doumanidis, C. Rebholz, The influence of structure on thermal behavior of reactive Al-Ni powder mixtures formed by ball milling, J. Alloys Compd. 505 (2010) 467–471. doi:10.1016/j.jallcom.2010.03.250.

[26] M. Aureli, C.C. Doumanidis, I.E. Gunduz, A.G.S. Hussien, Y. Liao, C. Rebholz, C.C. Doumanidis, Mechanics and energetics modeling of ball-milled metal foil and particle structures, Acta Mater. 123 (2017) 305–316. doi:10.1016/j.actamat.2016.10.041.

[27] Y. Saito, H. Utsunomiya, N. Tsuji, T. Sakai, Novel ultra-high straining process for bulk materials development of the accumulative roll-bonding (ARB) process, Acta Mater. 47 (1999) 579–583. doi:10.1016/S1359-6454(98)00365-6.

[28] L. Battezzati, P. Pappalepore, F. Durbiano, I. Gallino, Solid state reactions in Al/Ni alternate foils induced by cold rolling and annealing, Acta Mater. 47 (1999) 1901–1914. doi:10.1016/S1359-6454(99)00040-3.

[29] H. Sieber, J.S. Park, J. Weissmüller, J.H. Perepezko, Structural evolution and phase formation in cold-rolled aluminum-nickel multilayers, Acta Mater. 49 (2001) 1139–1151. doi:10.1016/S1359-6454(01)00023-4.

[30] S.W. Dean, J.K. Potter, R.A. Yetter, T.J. Eden, V. Champagne, M. Trexler, Energetic intermetallic materials formed by cold spray, Intermetallics. 43 (2013) 121–130.

doi:10.1016/j.intermet.2013.07.019.

[31] H. Zhao, C. Tan, X. Yu, X. Ning, Z. Nie, H. Cai, F. Wang, Y. Cui, Enhanced reactivity of Ni-Al reactive material formed by cold spraying combined with cold-pack rolling, J. Alloys Compd. 741 (2018) 883–894. doi:10.1016/j.jallcom.2018.01.170.

[32] A.P. Zhilyaev, T.G. Langdon, Using high-pressure torsion for metal processing: Fundamentals and applications, Prog. Mater. Sci. 53 (2008) 893–979. doi:10.1016/j.pmatsci.2008.03.002.

[33] A. Bachmaier, M. Kerber, D. Setman, R. Pippan, The formation of supersaturated solid solutions in Fe-Cu alloys deformed by high-pressure torsion, Acta Mater. 60 (2012) 860–871. doi:10.1016/j.actamat.2011.10.044.

[34] K. Edalati, S. Toh, M. Watanabe, Z. Horita, In situ production of bulk intermetallic-based nanocomposites and nanostructured intermetallics by high-pressure torsion, Scr. Mater. 66 (2012) 386–389. doi:10.1016/j.scriptamat.2011.11.039.

[35] X. Sauvage, P. Jessner, F. Vurpillot, R. Pippan, Nanostructure and properties of a Cu-Cr composite processed by severe plastic deformation, Scr. Mater. 58 (2008) 1125–1128. doi:10.1016/j.scriptamat.2008.02.010.

[36] S. Lee, K. Edalati, H. Iwaoka, Z. Horita, T. Ohtsuki, T. Ohkochi, M. Kotsugi, T. Kojima, M. Mizuguchi, K. Takanashi, Formation of FeNi with L10-ordered structure using high-pressure torsion, Philos. Mag. Lett. 94 (2014) 639–646. doi:10.1080/09500839.2014.955546.

[37] A. Alhamidi, K. Edalati, H. Iwaoka, Z. Horita, Effect of temperature on solid-state formation of bulk nanograined intermetallic Al3Ni during high-pressure torsion, Philos. Mag. 94 (2014) 876–887. doi:10.1080/14786435.2013.868945.

[38] A. Vorhauer, R. Pippan, On the onset of a steady state in body-centered cubic iron during severe plastic deformation at low homologous temperatures, Metall. Mater. Trans. A Phys. Metall. Mater. Sci. 39 (2008) 417–429. doi:10.1007/s11661-007-9413-1.

[39] A.P. Zhilyaev, T.G. Langdon, Using high-pressure torsion for metal processing: Fundamentals and applications, Prog. Mater. Sci. 53 (2008) 893–979. doi:10.1016/j.pmatsci.2008.03.002.

[40] K. Edalati, R. Miresmaeili, Z. Horita, H. Kanayama, R. Pippan, Significance of temperature increase in processing by high-pressure torsion, Mater. Sci. Eng. A. 528 (2011) 7301–7305. doi:10.1016/j.msea.2011.06.031.

[41] E. Ma, C. V. Thompson, L.A. Clevenger, K.N. Tu, Self-propagating explosive reactions in Al/Ni multilayer thin films, Appl. Phys. Lett. 57 (1990) 1262–1264. doi:10.1063/1.103504.

[42] F. Hausdorff, Dimension und äußeres Maß, Math. Ann. 79 (1918) 157–179. doi:10.1007/BF01457179.

[43] M. Reuter, Fraktaldimension von Grauwertbildern, University of Hannover, 1999.

[44] Int. Cent. Diffr. Data, Card Number 00-004-0850, Pdf-2/Release (2007), n.d.

[45] Int. Cent. Diffr. Data, Card Number 00-009-0097, Pdf-2/Release (2007), n.d.

[46] Int. Cent. Diffr. Data, Card Number 01-083-3994, Pdf-2/Release (2007), n.d.

[47] Int. Cent. Diffr. Data, Card Number 01-080-5811, Pdf-2/Release (2007), n.d.

[48] Int. Cent. Diffr. Data, Card Number 03-065-2418, Pdf-2/Release (2007), n.d.

[49] Int. Cent. Diffr. Data, Card Number 00-004-0787, Pdf-2/Release (2007), n.d.

[50] X. Sauvage, Y. Champion, R. Pippan, F. Cuvilly, L. Perrière, A. Akhatova, O. Renk, Structure and properties of a nanoscaled composition modulated metallic glass, J. Mater. Sci. 49 (2014) 5640–5645. doi:10.1007/s10853-014-8279-z.

[51] K.S. Kormout, R. Pippan, A. Bachmaier, Deformation-Induced Supersaturation in Immiscible Material Systems during High-Pressure Torsion, Adv. Eng. Mater. 19 (2017) 1600675. doi:10.1002/adem.201600675.

[52] I. Sabirov, R. Pippan, Characterization of tungsten fragmentation in a W-25%Cu composite after high-pressure torsion, Mater. Charact. 58 (2007) 848–853. doi:10.1016/j.matchar.2006.08.001.

[53] C.E. Shuck, M. Frazee, A. Gillman, M.T. Beason, I.E. Gunduz, K. Matouš, R. Winarski, A.S. Mukasyan, X-ray nanotomography and focused-ion-beam sectioning for quantitative three-dimensional analysis of nanocomposites, J. Synchrotron Radiat. 23 (2016) 990–996. doi:10.1107/S1600577516007992.

[54] B.B. Straumal, S.G. Protasova, A.A. Mazilkin, E. Rabkin, D. Goll, G. Schütz, B. Baretzky, R.Z. Valiev, Deformation-driven formation of equilibrium phases in the Cu-Ni alloys, J. Mater. Sci. 47 (2012) 360–367. doi:10.1007/s10853-011-5805-0.

[55] B.B. Straumal, A.R. Kilmametov, A. Korneva, A.A. Mazilkin, P.B. Straumal, P. Zięba, B. Baretzky, Phase transitions in Cu-based alloys under high pressure torsion, J. Alloys Compd. 707 (2017) 20–26. doi:10.1016/j.jallcom.2016.12.057.

[56] S.N. Arshad, T.G. Lach, M. Pouryazdan, H. Hahn, P. Bellon, S.J. Dillon, R.S. Averback, Dependence of shear-induced mixing on length scale, Scr. Mater. 68 (2013) 215–218. doi:10.1016/j.scriptamat.2012.10.027.

[57] X. Sauvage, G.P. Dinda, G. Wilde, Non-equilibrium intermixing and phase transformation in severely deformed Al/Ni multilayers, Scr. Mater. 56 (2007) 181–184. doi:10.1016/j.scriptamat.2006.10.021.

[58] A.J. Gavens, D. Van Heerden, A.B. Mann, M.E. Reiss, T.P. Weihs, Effect of intermixing on self-propagating exothermic reactions in Al/Ni nanolaminate foils, J. Appl. Phys. 87 (2000) 1255–1263. doi:10.1063/1.372005.

[59] S.C. Barron, S.T. Kelly, J. Kirchhoff, R. Knepper, K. Fisher, K.J.T. Livi, E.M. Dufresne, K. Fezzaa, T.W. Barbee, T.C. Hufnagel, T.P. Weihs, Self-propagating reactions in Al/Zr multilayers: Anomalous dependence of reaction velocity on bilayer thickness, J. Appl. Phys. 114 (2013) 223517. doi:10.1063/1.4840915.

[60] X. Qiu, J. Wang, Experimental evidence of two-stage formation of Al3Ni in reactive Ni/Al multilayer foils, Scr. Mater. 56 (2007) 1055–1058. doi:10.1016/j.scriptamat.2007.02.032.

[61] G.C. Pavlo Saltykov Lesley Cornish, Materials Science International Team, MSIT®, The assessed phase diagram of the Al-Ni system: Datasheet from MSI Eureka in SpringerMaterials (https://materials.springer.com/msi/phase-diagram/docs/sm{_}msi{_}r{_}20{_}010238{_}01{_}full{_}LnkDia0), (n.d.). https://materials.springer.com/msi/phase-

diagram/docs/sm_msi_r_20_010238_01_full_LnkDia0.

[62] G. Erdélyi, D.L. Beke, F.J. Kedves, I. Gödény, Determination of diffusion coefficients of Zn, Co and Ni in aluminium by a resistometric method, Philos. Mag. B Phys. Condens. Matter; Stat. Mech. Electron. Opt. Magn. Prop. 38 (1978) 445–462. doi:10.1080/13642817808246394.

[63] W. Gust, M.B. Hintz, A. Loddwg, H. Odelius, B. Predel, Impurity diffusion of Al in Ni single crystals studied by secondary ion mass spectrometry (SIMS), Phys. Status Solidi. 64 (1981) 187–194. doi:10.1002/pssa.2210640120.